Atmospheric pressure oxidation of Pt(111)

C Ellinger[1,4], A Stierle[1,4], I K Robinson[2], A Nefedov[3,5] and H Dosch[1]

[1] Max-Planck-Institut für Metallforschung, 70569 Stuttgart, Germany

[2] London Centre of Nanotechnology, London WC1H 0AH, UK

[3] Institut für Experimentalphysik/Festkörperphysik, Ruhr-Universität Bochum,
44780 Bochum, Germany

E-mail: stierle@mf.mpg.de

Abstract

The oxidation of the platinum (111) single crystal surface and the formation of platinum dioxide have been studied by *in situ* surface x-ray diffraction and x-ray reflectivity. At an oxygen partial pressure of 500 mbar and at temperatures from 520 to 910 K, the experiments disclose the growth of two atomic layers of a bulk-like, strongly distorted α-PtO$_2$. The epitaxial Pt oxide layer is oriented hexagon on hexagon with respect to the Pt(111) surface leading to a (8×8) superstructure surface unit cell. In a second set of experiments, a 100 Å thick epitaxial Pt(111) film on sapphire was exposed to oxygen. At 670 K and near atmospheric oxygen pressures we find the formation of a several angstrom thick oxide layer. After annealing the sample at 720 K in a vacuum the oxide layer desorbs, recovering the 100 Å thick Pt film. Subsequent oxidation at 720 K and reduction cycles lead to a slight increase in surface roughness and the formation of macroscopically visible holes in the Pt film. These results point to a Pt re-dispersion which sets in during chemical reactions at atmospheric pressures.

(Some figures in this article are in colour only in the electronic version)

Contents

1. Introduction

Pt and other transition metals like Ru and Pd are important industrial catalysts. In turn, a detailed microscopic understanding of their increased reactivity is necessary for further knowledge-based improvement of their catalytic functions. Recent studies [1–5] using partial oxygen pressures in the range of technologically important conditions have

shown that it is not the chemisorbed oxygen on the surfaces of Ru, Pd or Pt but rather the oxides formed on the surfaces which are believed to be most efficient for the oxidation of CO leading to an increased catalytic activity. This is in contrast to recent UHV based studies on Pd and Pt that have identified chemisorbed oxygen as the most active species [6, 7]. Pt belongs to the class of 'noble' metals like Au and Ag. Hence it remains rather stable even under highly reactive and corrosive conditions, maintaining its metallic shine due to the formation of a microscopically thin passivation layer. This also makes Pt attractive as a long life coating material for materials used in harsh working conditions, such as on the tips of spark plugs.

In order to understand the catalytic processes as well as the passivation of a transition metal surface covered by an oxide layer a few angstroms thick, it is necessary to study the formation, structure and stability of this oxide on the atomic scale. In the case of CO oxidation at open Pt(110) surfaces the following structures are observed under different applied conditions: an oxygen chemisorption structure and a thin commensurate and thin incommensurate oxide structure. These different states are accompanied by changes in catalytic activity [4, 5, 8]. At the close-packed Pt(111) surface, different oxygen chemisorption structures were determined for low

---

oxygen pressures [7]; in parallel possible oxide structures together with the increased reactivity of the CO/oxide/Pt—system have been investigated by density functional theory (DFT) [9].

In this report we show that an epitaxial Pt oxide layer is formed during the oxidation of a Pt(111) single crystal at atmospheric O_2 pressures. As we can infer from our *in situ* surface x-ray diffraction (SXRD) experiments, the layer is thicker than the oxygen–metal–oxygen trilayer surface oxides reported for Pd and Rh [10] and exhibits a strongly distorted α-PtO$_2$ structure in (0001) orientation. X-ray reflectivity experiments on a 100 Å thick, epitaxial grown Pt(111) film disclose the formation of a 4 Å thick oxide layer under high pressure conditions. An increase of the Pt film surface roughness and the formation of macroscopic holes is observed after an oxidation/reduction cycle at 720 K, most likely mediated by inhomogeneous material desorption from the film into the gas phase.

2. Experimental procedure

The Pt(111) single crystal was oriented better than 0.1° and chemically cleaned after polishing before insertion into the UHV chamber. Then the sample was cleaned by several annealing cycles up to 870 K for 30 min during oxygen exposures at 1×10^{-5} mbar, followed by a flash to 990 K under UHV conditions. Rocking curves in the minimum of the $(0, 1, L)$ crystal truncation rod (CTR) disclose a well ordered and clean surface after sample preparation. For the x-ray reflectivity studies, a 100 Å thick, sputter-deposited, epitaxial Pt(111) film on a single crystalline sapphire (11$\bar{2}$0) substrate was used [11]. The sample was cleaned by Ar ion sputtering followed by annealing to 720 K for 30 min. In both cases the sample was mounted on an Inconel sample holder with a temperature control of ± 10 K. Both *in situ* x-ray studies were performed in a UHV-compatible portable x-ray diffraction chamber which allows gas pressures from 10^{-10} mbar to 2 bar. The *in situ* SXRD study was performed at the MPI-MF beamline at the Angstrom Quelle Karlsruhe (ANKA), Germany [12], using a photon energy of 11.57 keV (wavelength $\lambda = 1.07$ Å). The experiments were carried out in six-circle diffraction mode with the incident angle fixed at the critical angle of Pt to optimize the signal to noise ratio. For the reflectivity experiments the oxidation chamber was mounted on a high resolution, two-circle diffractometer, using Mo Kα radiation ($\lambda = 0.71$ Å) from a 18 kW rotating anode.

3. Experimental results

3.1. Epitaxial growth of α-PtO$_2$

Pt has a face centred cubic structure ($a_0 = 3.924$ Å). For our experiment it is convenient to describe the structure in hexagonal coordinates as shown in figure 1. To investigate the growth of the oxide layer we performed K-scans at $H = 0$ and $L = 0.1$ reciprocal lattice units (figure 1(b)). In figure 2(a) a series of K-scans is plotted, recorded at a sample temperature of 520 K and an oxygen pressure of 500 mbar after different times. Besides the Pt crystal truncation rod (CTR) at $K = 1$
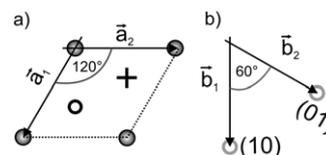
Figure 1. (a) Top view of the hexagonal surface unit cell of Pt(111): $a_1 = a_2 = 2.775$ Å, the lattice constant $a3$ perpendicular to the surface is 6.797 Å. Pt atoms in the surface are symbolized by the dark grey circles, the positions of the two other Pt atoms of lower layers are marked by the cross and the circle (ABC stacking). (b) Corresponding reciprocal space. The grey circles mark the position of the Pt CTRs.
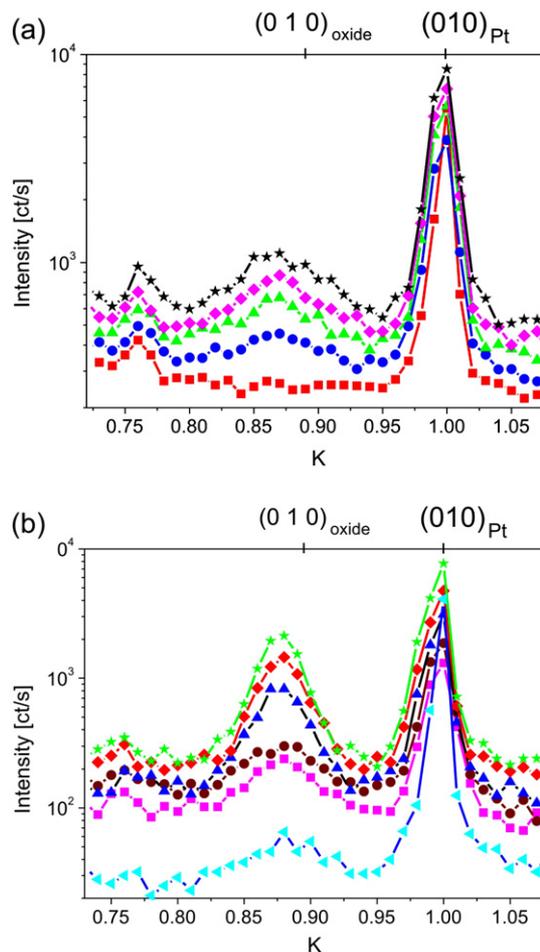
Figure 2. (Color online) (a) Time dependent K-scans during the oxidation of Pt(111) recorded 1 min, (red squares), 16 min (blue circles), 31 min (green triangles), 47 min (magenta rhombi) and 79 min (black stars) after an oxygen dose of 500 mbar at 520 K. A broad oxide peak is observed at $K = 0.88$. The vertical black line marks the (0,1,0) reflection position for bulk α-PtO$_2$. (b) Temperature dependent K-scans at 500 mbar O_2 pressure. The temperature was increased from 520 K (magenta squares), 600 K (brown circles), 770 K (blue, upward triangles), 840 K (red rhombi), 880 K (green stars) up to 910 K (turquoise, leftward triangles). In (a) and (b) the scans are offset in the y direction for clarity.

a new, broad peak arises at $K = 0.88$ which is assigned to an epitaxial oxide formed on the Pt(111) surface.

After 80 min of oxidation no further change was detected in the oxide peak intensity. The oxide film exhibits an average

domain size of 35 Å and a large mosaicity of $\Delta\theta = 12°$, as determined from rocking scans (rotation around the surface normal, not shown here) at a fixed momentum transfer of (0.88, 0, 0.1). This is even smaller than the Pt surface 'domain' size of 120 Å, measured by the width of the truncation rod. In order to increase the crystallinity of the layer, the sample was heated stepwise from 520 K up to 910 K at 500 mbar O_2 pressure (*K*-scans in figure 2(b)) leading in fact to a decrease in mosaicity from $\Delta\theta = 12°$ to 3°, and to an increase of the domain size to 60 Å. At 880 K and 500 mbar O_2 pressure, oxide desorption sets in and is completed at 910 K. The structural perfection of the oxide layer is very likely limited by kinetic barriers during the growth which explains why no ordered structures could be observed in a recent LEED study after oxidation at 450 K [7].

From the additionally observed oxide related diffraction peaks at (0.88, 0.88, 0.1) and (0.88, 0, 0.1) we conclude that the oxide has a hexagonal unit cell which is aligned parallel to the hexagonal unit cell of the Pt(111) substrate. Two stable bulk oxides are known for Pt, a CdI_2-like α-PtO_2 with a hexagonal unit cell [13, 14] and a $CaCl_2$-like β-PtO_2 [15, 16] with a tetragonal unit cell. From the in-plane peak position, we determine the in-plane lattice constant of the oxide to be $a_{oxide} = b_{oxide} = 3.15$ Å, which is close to the value of bulk platinum oxide α-PtO_2 ($a_{\alpha\text{-}PtO_2} = 3.10$ Å). Because of the hexagonal arrangement of the observed diffraction spots, we consider that our experimental results are consistent with the formation of hexagonal α-PtO_2.

3.2. 3D structure determination of the oxide layer

The full 3D structure of the oxide layer can be obtained with atomic resolution by a quantitative analysis of the Pt oxide surface rods. Figure 3 shows the modulus of the structure factor F of the (0, 0.88, L) and the (0.88, 0.88, L) oxide rod as a function of L (together with error bars resulting from statistical and systematic errors). For each data point the background-corrected integrated intensity has been measured by a rocking scan and corrected for standard six-circle geometry factors [17]. The solid and dashed lines in figure 3 represent the fitted structure factors for two different starting models [18], they are based on the structure of bulk α-PtO_2 with an in-plane lattice constant of 3.15 Å (figure 4(a)) and composed of one hexagonal Pt layer surrounded by oxygen (model I) or a full α-PtO_2 unit cell with two hexagonal Pt layers surrounded by oxygen (model II).

In the fit, the Pt atom positions were free, while the O atom positions were kept fixed relative to the Pt atoms at the bulk α-PtO_2-like positions. While the one-layer model (model I, dashed curve $\chi^2_{norm} = 6.1$), can clearly not reproduce the modulation of the measured data, the best fit was achieved with model II (solid curve, $\chi^2_{norm} = 2.9$). The associated structure (figure 4(b)) is a slightly modified bulk Pt oxide (α-PtO_2) with the top Pt oxide layer (light grey) shifted by $\sim 1/3$ unit cell along the [110] direction (see figure 4(b)). The Pt oxide layer in-plane lattice constant is 1.6% expanded, the out-of-plane lattice constant $c = 3.62$ Å is 15% reduced as compared with the bulk oxide values. The lateral displacement of the
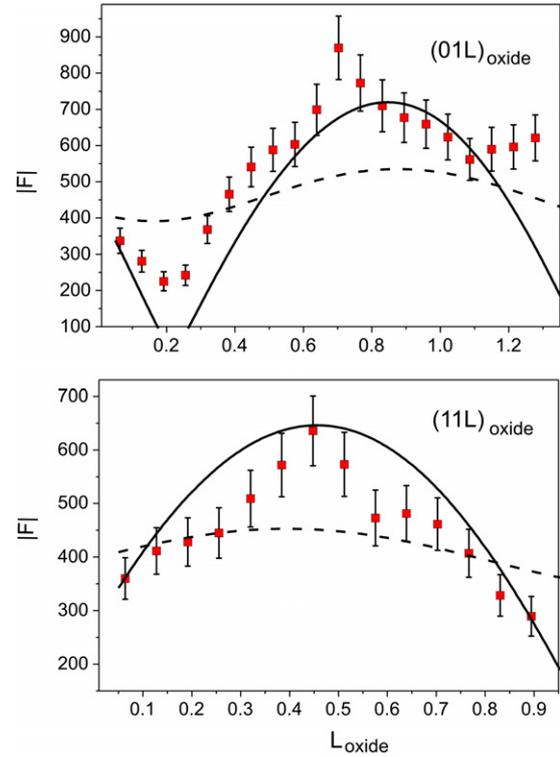
Figure 3. (01 *L*) and (11 *L*) surface rod of the oxide on Pt(111) in the reciprocal lattice coordinates of the hexagonal oxide unit cell. Open squares mark the experimental data with the corresponding error bars, the dashed and solid lines are fits from a structure model one and two Pt oxide layers thick (models I and II, respectively).
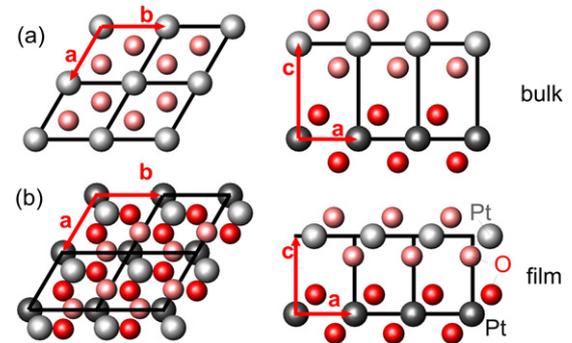
Figure 4. (a) Top and side view of the bulk oxide α-PtO_2 with lattice constants $a = b = 3.10$ Å and $c = 4.16$ Å and relative oxygen positions of (2/3, 1/3, 3/4) and (1/3, 2/3, 1/4) inside the unit cell. (b) Top and side views of the Pt oxide model obtained from a fit of the surface rods. The oxide layer consists of two Pt layers (light and dark grey spheres represent Pt atoms, red (smaller) spheres oxygen atoms) with a compressed c axis lattice constant as compared to α-PtO_2.

topmost Pt oxide layer must be responsible for this remarkable reduction of the c lattice constant. Such a lateral shift is not expected to be energetically costly, because the Pt layers of α-PtO_2 are only weakly bound by van der Waals forces in the c-direction [8]. Note that the shift does not conserve the P3 M1 symmetry of the bulk oxide structure. As our fit is not compatible with domain formation, we are forced to conclude that oxide formation is initiated at step edges.
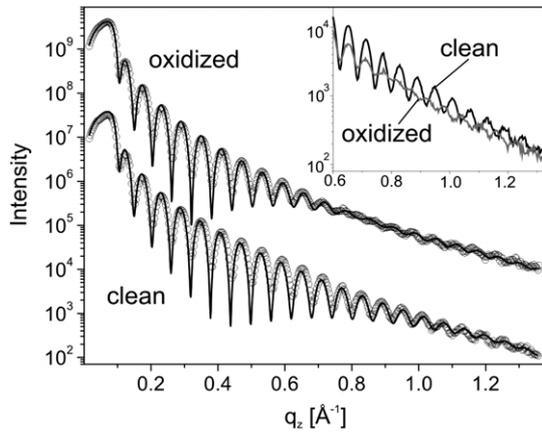
Figure 5. Specular reflected intensity (open circles) and corresponding fits (solid lines) as a function of the magnitude of the scattering vector $q_z = (4\pi/\lambda)\sin\theta$ perpendicular to the surface (θ represents the grazing angle and λ the x-ray wavelength). Upper curve, clean surface at 570 K; lower curve, 570 K and 512 mbar oxygen pressure. The two curves are shifted relative to each other by a factor of 100 for clarity. The inset shows the region of $q_z = 0.84\,\text{Å}^{-1}$ to highlight the oxide layer induced beating.

3.3. In situ x-ray reflectivity measurements

In a second set of experiments the stability and integrity of epitaxial Pt films on sapphire substrates was monitored under oxidizing conditions. The use of thin films allows us to get more precise information on material transport and loss during Pt oxidation experiments. Specular reflected x-ray intensity distributions provide information on the average electron density profile normal to the surface, which is characteristically changing during the oxidation process [19, 20]. After cleaning the sample as described above, a reflectivity measurement was performed at 570 K under UHV conditions (lower curve in figure 5). The observed intensity oscillations are directly related to the Pt film thickness and interfacial roughness which are determined to be 102 Å (± 1 Å) as well as 2 Å (± 0.2 Å) (vac/Pt interface) and 1 Å (± 0.1 Å) (Pt/sapphire interface), respectively.

The Pt film was subsequently oxidized at 570 K and 500 mbar. The reflected intensity was measured under oxygen exposure, 1 h after the introduction of O_2. The data and the fit are shown in figure 5 (upper curve). In addition to the thickness oscillations from the Pt film, a beating is observable with a minimum at $q_z = 0.84\,\text{Å}^{-1}$ (see also the inset of figure 5). This indicates clearly that a layer with different density has grown on the Pt film, which we can identify as the oxide layer. The best fit provides an additional layer with a thickness of 4 Å and a total electron density close to that of the Pt oxide layer described above. Due to this oxidation process the thickness of the Pt film was reduced slightly to 99 Å. The roughnesses from the vacuum/oxide, the oxide/Pt and the Pt/sapphire interfaces showed very low values similar to the unoxidized film. To restore a clean sample, the Pt film was annealed in UHV at 720 K for 30 min which led to a desorption of the oxide.

This oxidation cycle was repeated for different sample temperatures. Up to 670 K the situation is very similar to the
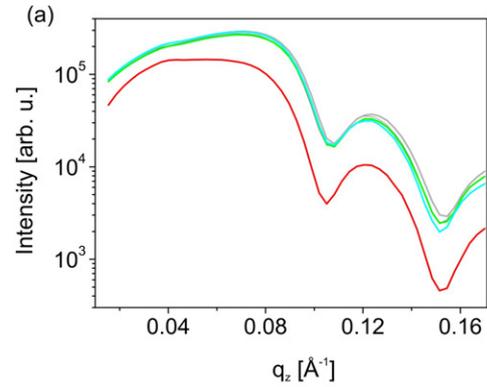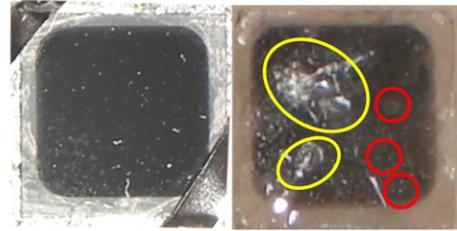
Figure 6. (a) Specular reflected intensities close to q_c from the clean sample after oxidation/reduction cycles at 512 mbar O_2 pressure. The upper three curves have been obtained in the temperature range from 570 to 670 K, the lower after oxidation at 720 K. (b) Left: photograph of a 100 Å thick Pt film on sapphire treated by several heating cycles up to 720 K under UHV conditions. Right: photograph of the sample after the oxygen treatment at 500 mbar and 720 K. Macroscopic defects are visible, along with discoloration of the outlying sapphire substrate.

one described above. Finally, at 720 K, a loss of half of the specular reflected intensity was observed (figure 6(a)), which is in line with a partial desorption or macroscopic roughening of the film. As the Pt film thickness of 102 Å remains constant, we assume that the material loss occurs locally at impurities or defects. We note that macroscopic holes are observable in the Pt film after the oxidation treatment (see photograph in figure 6(b)). The sample also shows a discoloration of the laterally extending sapphire substrate (figure 6(b), right), probably due to Pt or Pt oxide re-dispersion. For comparison, in figure 6(a) a photograph of a 100 Å thick Pt film grown on sapphire is given, which was treated by the same annealing cycles up to 720 K but under UHV conditions. As no heat induced material loss could be detected on this second sample, we conclude that the observed Pt material loss is induced by the interaction with oxygen at elevated pressures.

4. Discussion and conclusions

We have disclosed that α-PtO_2 grows in a hexagon-on-hexagon arrangement on the (111) surface. Because of the nominally large misfit of 13.5%, this is a rather surprising observation. Note here that the misfit of an oxide film in a c(2 × 2) arrangement (rotated by 30° with respect to the experimentally observed in-plane orientation) would result in only 1.7% misfit, in turn an energetically more stable
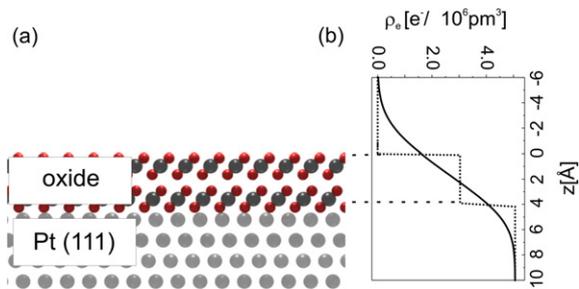
Figure 7. (a) Side view of the platinum oxide on Pt(111) along the [1,1,$\bar{2}$] direction: structural model as determined from SXRD. (b) Electron density profile $\rho_e(z)$ obtained from the fit of the reflectivity curve. The dashed line represents the electron density profile without roughness. The dark grey spheres represent Pt atoms in the oxide layer, light grey spheres Pt atoms in the metal substrate. Oxygen atoms are plotted as small (red) spheres.

interface should be formed as put forward by a recent density functional theory calculation [8]. Nevertheless, the in-plane oxide lattice constant of 3.15 Å is very close to a (8×8) coincidence structure on top of the Pt(111) substrate. Since we found no experimental evidence for the formation of an oxide layer in a $c(2 \times 2)$ orientation, we consider that the $p(8 \times 8)$ coincidence structure takes precedence. We note that a similar situation is also observed for other hexagonal interfaces like $Ag_2O(111)$ on Ag(111), Ag(111) on ZnO(0001) and $Cu_2O(111)$ on Cu(111) [21–23]. The origin for the stability of this seemingly unfavourable alignment between the oxide layer and the metal substrate might be found in the local bonding at the metal–oxide interface, giving rise to an increased number of metal–oxygen bonds, as compared with the $c(2 \times 2)$ arrangement.

The x-ray data allow us to construct a full 3D model of the interface, as shown in figure 7. The compression of the oxide layer in the c direction is in line with the observation of such a compressed α-PtO_2 layer on the Pt(110) surface [1]. The total electron density that we deduce for the layer is 17% higher than for bulk α-PtO_2. From a comparison of the reflectivity density profile and the structure of the oxide layer, it becomes apparent that oxygen might be located at the metal–oxide interface. The oxide layer involves two metal layers, in contrast to metal–oxygen–metal trilayer surface oxides, which form on other late transition metal surfaces, like Pd and Rh [9].

As both the reflectivity and the surface rod results yield a similar electron density for the oxide layer, we conclude that the surface is fully covered by the oxide layer. Such an ultrathin oxide layer is believed to serve as an oxygen reservoir during chemical reactions, like CO oxidation [4]. In addition the reflectivity measurements give evidence for an oxygen induced material re-dispersion starting at 720 K and oxygen pressures of 112 mbar accompanied by a partially irreversible

surface roughening. This unwanted material transport may have important consequences for the use of Pt as a catalyst material or as a protective coating.

Acknowledgments

References

[1] Over H, Kim Y D, Seitsonen A P, Wendt S, Lundgren E, Schmid M, Varga P, Morgante A and Ertl G 2000 *Science* **287** 1474
[2] Hendriksen B L M, Bobaru S C and Frenken J W M 2004 *Surf. Sci.* **552** 229
[3] Hendriksen B L M and Frenken J W M 2002 *Phys. Rev. Lett.* **89** 046101
[4] Ackermann M D, Pedersen T M, Hendriksen B L M, Robach O, Bobaru S C, Popa I, Quiros C, Kim H, Hammer B, Ferrer S and Frenken J W M 2005 *Phys. Rev. Lett.* **95** 255505
[5] Li W X, Oesterlund L, Vestergaard E K, Vang R T, Matthiesen J, Pedersen T M, Lægsgaard E, Hammer B and Besenbacher F 2004 *Phys. Rev. Lett.* **93** 146104
[6] Zheng E and Altman E I 2002 *J. Phys. Chem.* B **106** 1048
[7] Weaver J F, Chen J-J and Gerrad A L 2005 *Surf. Sci.* **592** 83
[8] Pedersen T M, Li W X and Hammer B 2006 *Phys. Chem. Chem. Phys.* **8** 1566–74
[9] Li W X and Hammer B 2005 *Chem. Phys. Lett.* **409** 1
[10] Lundgren E, Mikkelsen A, Andersen J N, Kresse G, Schmid M and Varga P 2006 *J. Phys.: Condens. Matter* **18** R481
[11] Nefedov A, Abromeit A, Morawe C and Stierle A 1998 *J. Phys.: Condens. Matter* **10** 717
[12] Stierle A, Steinhaeuser A, Ruehm A, Renner F U, Weigel R, Kapser N and Dosch H 2004 *Rev. Sci. Instrum.* **75** 5302
[13] Weber W H, Graham G W and McBridge J R 1990 *Phys. Rev.* B **42** 10969
[14] Hoekstra H R, Siegel S and Gallagher F X 1971 *Adv. Chem. Ser.* **98** 39
[15] McBridge J R, Graham G W, Peters C R and Weber W H 1991 *J. Appl. Phys.* **69** 3
[16] Range K J, Rau F, Klement U and Heyns A M 1987 *MRS Bull.* **22** 1541
[17] Vlieg E 1997 *J. Appl. Crystallogr.* **30** 532
[18] Vlieg E 2000 *J. Appl. Crystallogr.* **33** 401
[19] Parratt L G 1954 *Phys. Rev.* **2** 95
[20] Nevot L and Croce P 1980 *Rev. Phys. Appl.* **15** 761
[21] Reicho A, Stierle A, Costina I and Dosch H 2007 *Surf. Sci.* **601** L19
[22] Jedrecy N, Renaud G, Lazzari R and Juppille J 2005 *Phys. Rev.* B **72** 045430
[23] Chu Y S, Robinson I K and Gewirth A A 1999 *J. Chem. Phys.* **110** 5952